

# Thermal conductivity of $\text{AlAs}_{0.07}\text{Sb}_{0.93}$ and $\text{Al}_{0.9}\text{Ga}_{0.1}\text{As}_{0.07}\text{Sb}_{0.93}$ alloys and $(\text{AlAs})_1/(\text{AlSb})_{11}$ digital-alloy superlattices

T. Borca-Tasciuc<sup>a)</sup>

*Department of Mechanical, Aerospace, and Nuclear Engineering, Rensselaer Polytechnic Institute, Troy, New York 12180*

D. W. Song

*Department of Mechanical and Aerospace Engineering, University of California, Los Angeles, California 90095*

J. R. Meyer, I. Vurgaftman, M.-J. Yang, B. Z. Nosho<sup>b)</sup>, and L. J. Whitman

*Naval Research Laboratory, Washington DC 20375*

H. Lee and R. U. Martinelli

*Sarnoff Corporation, Princeton, New Jersey 08543*

G. W. Turner and M. J. Manfra

*MIT Lincoln Laboratory, Lexington, Massachusetts 02173*

G. Chen

*Department of Mechanical Engineering, Massachusetts Institute of Technology, Boston, Massachusetts 02139*

(Received 6 May 2002; accepted 17 July 2002)

A differential  $3\omega$  technique is employed to determine the thermal conductivity of the  $\text{AlAs}_{0.07}\text{Sb}_{0.93}$  ternary alloy, the  $\text{Al}_{0.9}\text{Ga}_{0.1}\text{As}_{0.07}\text{Sb}_{0.93}$  quaternary alloy, and an  $(\text{AlAs})_1/(\text{AlSb})_{11}$  digital-alloy superlattice. Between 80 and 300 K, the thermal conductivities for all three samples are relatively insensitive to temperature. The thermal conductivity of the  $(\text{AlAs})_1/(\text{AlSb})_{11}$  superlattice is smaller than that of the  $\text{AlAs}_{0.07}\text{Sb}_{0.93}$  ternary alloy, but much larger than the predictions of a model for phonon transport across the superlattice interfaces. © 2002 American Institute of Physics.

[DOI: 10.1063/1.1506194]

## INTRODUCTION

The antimonide family of III–V heterostructure materials with lattice constants near  $6.1 \text{ \AA}$  has become increasingly important as the basis for electronic and optoelectronic devices such as high-speed field effect transistors, infrared lasers, infrared photodetectors, and thermophotovoltaics.<sup>1–8</sup> Besides the binaries GaSb, InAs, and AlSb, this family includes a number of ternary ( $\text{Ga}_{1-x}\text{In}_x\text{Sb}$ ,  $\text{AlAs}_x\text{Sb}_{1-x}$ , etc.) and quaternary ( $\text{Ga}_{1-x}\text{In}_x\text{As}_y\text{Sb}_{1-y}$ ,  $\text{Al}_x\text{Ga}_{1-x}\text{As}_y\text{Sb}_{1-y}$ , etc.) random alloys,<sup>9</sup> as well as superlattices (e.g., InAs/AlSb, InAs/ $\text{Ga}_{1-x}\text{In}_x\text{Sb}$ ) and digital alloys (e.g.,  $\text{Ga}_{1-x}\text{In}_x\text{As}/\text{Ga}_{1-x}\text{In}_x\text{Sb}$ , AlAs/AlSb) that provide numerous additional opportunities for engineering of the band structures and electronic wave functions.

Thermal conductivity  $\kappa$  is a key parameter in many device applications. This is particularly true of lasers, which generate considerable quantities of heat that must be dissipated. While the thermal conductivities of GaSb, AlSb, and InAs are well known,<sup>10</sup> few data are currently available for the various antimonide random alloys, digital alloys, and superlattices. It is known that the thermal conductivity of other III–V alloys such as  $\text{Al}_x\text{Ga}_{1-x}\text{As}$  are lower than the binary

endpoints,<sup>11</sup> which is attributed to alloy-disorder scattering induced by strain and mass-point defects.<sup>12</sup> Although thermal conductivities have also been reported for the quaternaries  $\text{Al}_{0.1}\text{Ga}_{0.9}\text{As}_{0.52}\text{Sb}_{0.48}$  (Ref. 13) (matched to InP) and  $\text{Al}_x\text{Ga}_{1-x}\text{As}_y\text{Sb}_{1-y}$  (Ref. 14) with  $x=0-0.5$  and lattice matched to GaSb, no previous data are available for  $\text{Al}_x\text{Ga}_{1-x}\text{As}_y\text{Sb}_{1-y}$  with high Al concentrations.

Thermal conductivities in superlattices such as GaAs/Al(Ga)As,<sup>15–18</sup> InAs/AlSb<sup>19</sup> and InP/InGaAs<sup>20</sup>, are much lower than the predictions based on Fourier law and bulk thermal conductivity values of their constituents, and tend to be even lower than in alloys with the same average composition. Various models based on minigap scattering,<sup>21</sup> the Boltzmann transport equation,<sup>22,23</sup> and phonon group velocity reduction<sup>24–26</sup> have been developed to explain this trend. The only previously published thermal conductivity measurements for antimonide superlattices [InAs/AlSb ( $33 \text{ \AA}/32 \text{ \AA}$ )] found cross-plane thermal conductivity values that were a full 1 order of magnitude lower than the bulk values for both InAs and AlSb.<sup>19</sup> The implication is that such layers, which have been employed frequently in the injection regions of antimonide mid-infrared lasers,<sup>27,28</sup> should be avoided from the thermal management standpoint. Since ternary  $\text{AlAs}_x\text{Sb}_{1-x}$  or quaternary  $\text{Al}_x\text{Ga}_{1-x}\text{As}_y\text{Sb}_{1-y}$  can provide alternative injection regions,<sup>4</sup> it is important to determine the thermal conductivity for those alloys. A second configuration of interest is the “digital alloy”<sup>29,30</sup>, in which

<sup>a)</sup>Author to whom correspondence should be addressed; electronic mail: borcat@rpi.edu

<sup>b)</sup>Permanent address: HRL Laboratories, LLC, Malibu, CA 90265.

constituent layers may be as thin as 1 monolayer (ML). One must be concerned by the general decrease of the thermal conductivity with decreasing superlattice period that most GaAs/Al(Ga)As experiments have observed.<sup>15,18</sup> A decrease into the ultrashort-period limit would imply that digital alloys are also very detrimental to the heat removal in high-duty-cycle devices. However, one recent theory predicts the presence of a minimum followed by an increase of  $\kappa$  at the shortest periods.<sup>25</sup> Earlier modeling results<sup>24,31</sup> show similar trends in short period superlattices, although these studies did not predict the increasing thermal conductivity in thicker superlattices. There have been no previous thermal conductivity experiments on III–V digital alloys.

In the present work we used a differential  $3\omega$  technique, in conjunction with a multilayer two-dimensional heat conduction model, to measure temperature-dependent thermal conductivities for three antimonide-based materials: an AlAs<sub>0.07</sub>Sb<sub>0.93</sub> ternary alloy, an Al<sub>0.9</sub>Ga<sub>0.1</sub>As<sub>0.07</sub>Sb<sub>0.93</sub> quaternary alloy, and an (AlAs)<sub>1</sub>/(AlSb)<sub>11</sub> superlattice digital alloy, all of which have an average lattice constant near that of GaSb. While each of these materials is important individually as a key constituent of lasers and other potential device structures, it is also instructive to compare the three results. It will be seen that the thermal conductivity of the digital alloy is considerably higher than might have been expected from an extrapolation of earlier theory and data.

## SAMPLE AND MEASUREMENT TECHNIQUE

The three undoped films were grown by molecular beam epitaxy at three different facilities. All were grown on GaSb substrates and protected by thin GaSb cap layers ( $\approx 100$  Å). The AlAs<sub>0.07</sub>Sb<sub>0.93</sub> ternary alloy (MIT Lincoln Laboratory) was 0.62  $\mu\text{m}$  thick, and its composition was confirmed by x-ray rocking-curve data. The Al<sub>0.9</sub>Ga<sub>0.1</sub>As<sub>0.07</sub>Sb<sub>0.93</sub> quaternary alloy (Sarnoff) was 1.3  $\mu\text{m}$  thick. The digital alloy (NRL) comprised 280 repeats of an (AlAs)<sub>1</sub>/(AlSb)<sub>11</sub> superlattice, for a total thickness of 1.02  $\mu\text{m}$ .

The layer abruptness of a representative (AlAs)<sub>1</sub>/(AlSb)<sub>11</sub> digital alloy, grown under similar conditions to the thermal conductivity sample, was characterized by cross-sectional scanning tunneling microscopy (XSTM). This technique provides an “edge-on,” atomic-scale, cross-sectional view of a {110} cleavage face. The XSTM image in Fig. 1 shows the filled electronic states on the (110) surface, revealing the anion lattice (As/Sb) of every other layer grown.<sup>32</sup> In this gray-scale image, As atoms appear darker than Sb, principally because of the shorter bond length of the AlAs versus AlSb.<sup>32</sup> The image demonstrates that the As is well confined, with relatively little interdiffusion into the 11 AlSb layers between each AlAs layer, and has not formed a random alloy. Quantitatively, the observation that the AlAs is confined primarily to a single XSTM layer/period implies that its actual distribution is spread over no more than 2 growth MLs/period (since only every other growth layer is exposed in the image).

A differential  $3\omega$  method was employed to measure the cross-plane thermal conductivities of the three films. In the

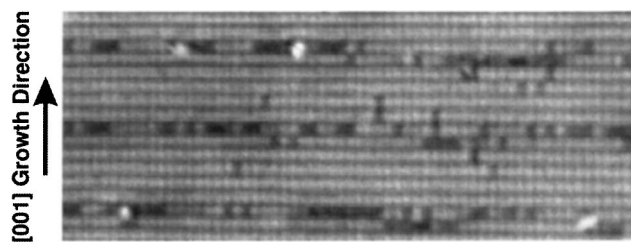


FIG. 1. XSTM image of a representative (AlAs)<sub>1</sub>/(AlSb)<sub>11</sub> digital-alloy superlattice. In this 26.5 nm $\times$ 10.4 nm gray-scale image, As atoms appear darker than Sb. The AlAs appears to be well confined, with relatively little interdiffusion into the adjacent AlSb layers.

$3\omega$  method,<sup>33</sup> a metallic wire is deposited onto the sample to act as both a heater and temperature sensor when modulated current passes through it. Since the measured films are semi-conducting, the wire must be electrically insulated from the sample surface to avoid current leakage. The electrical insulation was provided by thin (83–100 nm) Si<sub>x</sub>N<sub>y</sub> films deposited onto the samples by plasma enhanced chemical vapor deposition at 150 °C. In the differential  $3\omega$  method, the temperature drop across the film of interest is measured experimentally by taking the difference in temperature rise between similar heaters deposited on the sample and a reference without the film. The experiments are carried out over a frequency range where the measured temperature drop is frequency independent. The thermal conductivity of the film is extracted from the best fit between the measured temperature drop and predictions of a heat conduction model, using the unknown thermal conductivity of the film as a fitting parameter. Since heat spreading and effects associated with the substrate/film thermal-conductivity contrast must be taken into account for this configuration,<sup>34</sup> a two-dimensional heat conduction model<sup>34,35</sup> was used. The fitting also employed experimentally measured values for the thermal conductivity of the substrate and Si<sub>x</sub>N<sub>y</sub>, which were determined by fitting the frequency dependent temperature rise of the heater deposited on the reference sample. The advantage of the differential technique is that the measured thermal conductivity of the film of interest is relatively less affected by uncertainties associated with the thermal properties of the substrate and insulation layer.

The experiments were carried out at temperatures between 80 and 300 K. Calibration of the temperature coefficient of resistance for the metallic wires was performed during the slow warmup of the cryostat. The  $3\omega$  voltage was measured by a lock-in amplifier, and the data acquisition and control were computer automated.

## EXPERIMENTAL RESULTS AND DISCUSSION

Figure 2 shows examples of the experimental (points) frequency-dependent temperature amplitude measured at 80 and 300 K, for the case of 10- $\mu\text{m}$ -wide heaters deposited on the GaSb substrate reference and the Al<sub>0.9</sub>Ga<sub>0.1</sub>As<sub>0.07</sub>Sb<sub>0.93</sub> quaternary alloy film. The temperature difference measured between the sample S and the substrate reference R, which is constant over this frequency range, is used to determine the thermal conductivity of the alloy film. The curves in Fig. 2

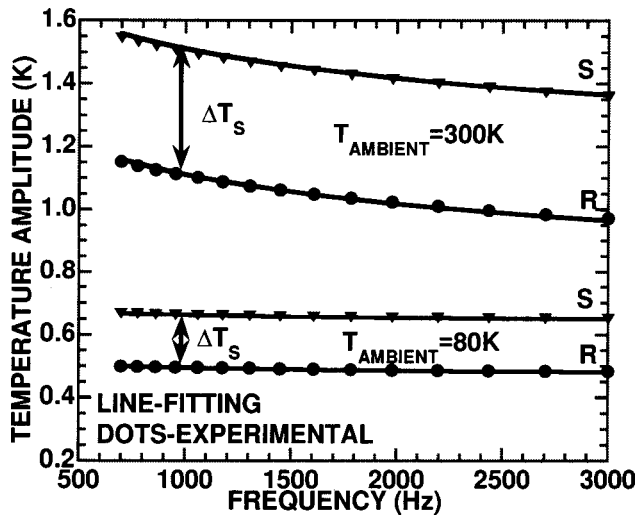


FIG. 2. Experimental temperature amplitude as a function of modulation frequency, measured at 80 and 300 K for 10  $\mu\text{m}$  heaters and temperature sensors deposited on the reference GaSb substrate R and on the  $\text{Al}_{0.9}\text{Ga}_{0.1}\text{As}_{0.07}\text{Sb}_{0.93}$  quaternary alloy sample S.

show the modeled heater temperature rise using fitted values for the thermal conductivities of the substrate, insulation layer, and alloy film.

The temperature-dependent cross-plane thermal conductivities are shown in Fig. 3 for all three films:  $\text{AlAs}_{0.07}\text{Sb}_{0.93}$  (boxes),  $\text{Al}_{0.9}\text{Ga}_{0.1}\text{As}_{0.07}\text{Sb}_{0.93}$  (crosses), and the  $(\text{AlAs})_1/(\text{AlSb})_{11}$  superlattice (triangles). The experimental uncertainty of the measured thermal conductivity is  $\sim 20\%$  for the ternary alloy film and  $\sim 10\%$  for the quaternary alloy and superlattice films. The thermal conductivities of binary III–V compounds typically peak at 10–30 K and have a  $1/T^n$

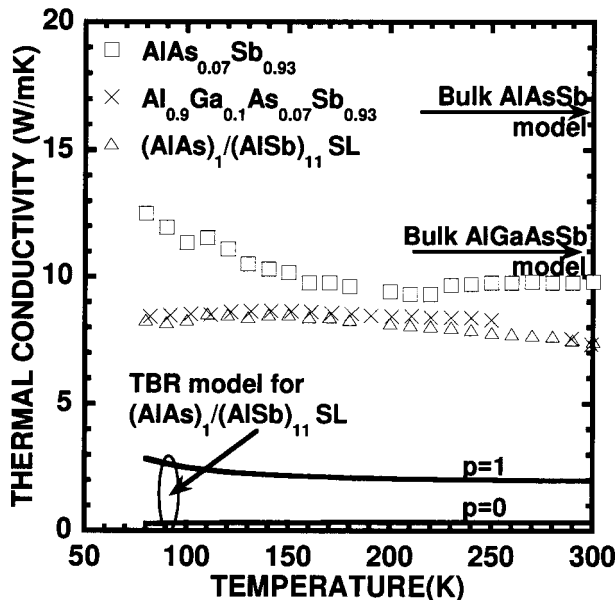


FIG. 3. Temperature-dependent thermal conductivities of the three films. The experimental results (points) are compared with predictions for the bulk thermal conductivity of the alloys at room temperature (arrows) and of the superlattice (curves) assuming upper ( $p=1$  means specular scattering) and lower ( $p=0$  means diffuse scattering) limits on the specularly of the phonon scattering at the superlattice interfaces.

TABLE I. Comparison of thermal conductivities at 300 K from this work with earlier related results.

	Lattice match	$\kappa$ (300 K) (W/mK)	Reference
AlSb	...	57	10
AlAs	...	91	10
GaSb	...	33	10
$\text{AlAs}_{0.56}\text{Sb}_{0.44}$	InP	4.2	10
$\text{Al}_{0.1}\text{Ga}_{0.9}\text{As}_{0.52}\text{Sb}_{0.48}$	InP	3.2	13
$(\text{InAs})_{11}/(\text{AlSb})_{10}\text{SL}$	GaSb	2.7–3.3	19
$\text{Al}_{0.2}\text{Ga}_{0.8}\text{As}_{0.02}\text{Sb}_{0.98}$	GaSb	18.2	14
$\text{Al}_{0.27}\text{Ga}_{0.73}\text{As}_{0.03}\text{Sb}_{0.97}$	GaSb	10.5	14
$\text{Al}_{0.51}\text{Ga}_{0.49}\text{As}_{0.05}\text{Sb}_{0.95}$	GaSb	7.7	14
$\text{Al}_{0.9}\text{Ga}_{0.1}\text{As}_{0.09}\text{Sb}_{0.93}$	GaSb	7.1	this work
$\text{AlAs}_{0.07}\text{Sb}_{0.93}$	GaSb	9.8	this work
$(\text{AlAs})_1/(\text{AlSb})_{10}$	GaSb	7.3	this work

dependence (with  $n=1-1.5$ ) in the 80–300 K range. By comparison, the studied films have a much weaker dependence on temperature, as is typical when mechanisms other than phonon–phonon scattering dominate the thermal transport. Moreover, the thermal conductivities are much lower than those of the binary  $(\text{Al,Ga})/(\text{As,Sb})$  compounds. This may be seen from Table I, which compares the present results at 300 K with earlier data for related binaries, ternaries, quaternaries, and superlattices. For example at 300 K, the thermal conductivities of the binaries range between 33 W/mK for GaSb to 91 W/mK for AlAs,<sup>36</sup> while the corresponding values measured in the present experiments are  $\sim 10$  W/mK for the ternary alloy, and  $\sim 7$  W/mK for the quaternary alloy and the superlattice.

For comparison, Fig. 3 also shows theoretical predictions for the two alloys at room temperature (arrows) and for the superlattice as a function of temperature (curves). The theory for bulk alloys at  $T$  above the Debye temperature is taken from the phenomenological model of Abeles,<sup>12</sup> which includes normal and Umklapp three-phonon anharmonic processes as well as alloy-disorder scattering induced by strain and mass-point defects. The calculation employs an interpolation scheme<sup>10,36,37</sup> based on the thermal resistivities of the binary compounds along with nonlinear contributions (bowing parameters) associated with the random distribution of atoms on the sublattice sites. The binary thermal resistivities and values for the bowing parameters are taken from Ref. 10. The predicted room-temperature thermal conductivities for  $\text{AlAs}_{0.07}\text{Sb}_{0.93}$  and  $\text{Al}_{0.9}\text{Ga}_{0.1}\text{As}_{0.07}\text{Sb}_{0.93}$  are 15 and 11 W/mK, respectively, whereas both measured values are  $\approx 65\%$  of the respective predictions. Three possible explanations for the measured thermal conductivity reduction are discussed below. Since the present samples are actually thin films (0.62 and 1.3  $\mu\text{m}$ ), size effects due to the interface scattering of long-wavelength phonons may have contributed to a reduction of  $\kappa$ . However, this explanation is probably unlikely in the view of a recent experimental report,<sup>38</sup> indicating the dominance of alloy scattering mechanisms in the thermal conductivity reduction of SiGe alloy superlattices. Another possibility is that the theoretically derived bowing parameter for AlAsSb needs to be adjusted upward. This procedure would lead to much better agreement with theory

for both the ternary and quaternary alloys, since the AlAsSb bowing affects the thermal resistance in both. The present measurements imply a thermal-resistivity bowing parameter of 130 cm K/W. The earlier data in Ref. 13 are consistent with values nearly as high, in the 90–100 cm K/W range, whereas the theoretical value from Ref. 10 is 65 cm K/W. The most likely explanation for the measured thermal conductivity reduction is based on the interface thermal resistance between the measured films and the GaSb substrate. The film–substrate interface thermal resistance is not subtracted by the differential measurement technique, and therefore is included in the measured thermal resistance of the film. Comparing the predicted thermal resistance of the alloy films with the experimental values measured at room temperature, the interface thermal resistance is estimated to be  $\sim 2.1 \times 10^{-8} \text{ K m}^2 \text{ W}^{-1}$  for the ternary alloy and  $\sim 6.8 \times 10^{-8} \text{ K m}^2 \text{ W}^{-1}$  for the quaternary alloy. These values are of the same order of magnitude as measured for the interface thermal resistance between dielectric films and Si substrate.<sup>39</sup> However, additional measurements, e.g., on bulk alloy layers or on films with different thicknesses, are needed to resolve which of the three mechanisms are responsible for the measured thermal conductivity reduction in the alloy layers.

One model for thermal transport in superlattices is based on the thermal boundary resistance (TBR) at the interface between two adjacent layers.<sup>40</sup> The phonon transmissivity at each interface depends on such material parameters as the density, specific heat, bulk thermal conductivity, and phonon spectra, as well as the specular parameter  $p$ . That parameter represents the fraction of phonons impinging on the interface that are scattered specularly (reflected and transmitted), hence its value must be between  $p=0$  (totally diffuse) and  $p=1$  (totally specular). The temperature-dependent theory curves in Fig. 3, which correspond to both of those limits, indicate that the thermal conductivity derived from the TBR model for the  $(\text{AlAs})_1/(\text{AlSb})_{11}$  digital-alloy superlattice is too small by almost 1 order of magnitude. A possible explanation for this discrepancy is phonon tunneling, which may contribute significantly to the heat transfer across 1–2 ML of AlAs. The increase of heat transport across very thin superlattice layers was predicted by models based on the phonon-wave approach, such as lattice dynamics simulations<sup>24,25</sup> and acoustic wave propagation across superlattice interfaces.<sup>31</sup>

Thus while  $\kappa$  for the digital-alloy superlattice is considerably smaller than the bulk binary values, as expected, it is only moderately lower than that for the random alloy with the same average composition. And significantly, it is much higher than one would obtain from an extrapolation of the phonon transport models for thicker-period superlattices to the short-period limit, which is consistent with recent theoretical predictions.<sup>24,25,31</sup> Of course, the XSTM results (Fig. 1) clearly show that the present structure does not represent a perfect digital-alloy superlattice with the As atoms confined strictly to a single monolayer.

## CONCLUSIONS

The thermal conductivities of ternary  $\text{AlAs}_{0.07}\text{Sb}_{0.93}$ , quaternary  $\text{Al}_{0.9}\text{Ga}_{0.1}\text{As}_{0.07}\text{Sb}_{0.93}$ , and  $(\text{AlAs})_1/(\text{AlSb})_{11}$

digital-alloy superlattice films have been measured between 80 K and room temperature. Over this range the observed  $\kappa$  are nearly independent of  $T$ , since mechanisms other than phonon-phonon scattering dominate the thermal transport. At room temperature the thermal conductivities of the alloys are  $\approx 35\%$  smaller than the values expected from a bulk model. The most likely explanation for the measured thermal conductivity reduction is the existence of a small ( $2.1\text{--}6.8 \times 10^{-8} \text{ K m}^2 \text{ W}^{-1}$ ) interface thermal resistance between the alloy films and the GaSb substrate. The thermal conductivity of the  $(\text{AlAs})_1/(\text{AlSb})_{11}$  superlattice is 30% smaller than that of the  $\text{AlAs}_{0.07}\text{Sb}_{0.93}$  alloy, despite similar average compositions. However, the superlattice result exceeds considerably the thermal conductivity predicted by a theory for the thermal boundary resistance across superlattice interfaces, possibly due to phonon tunneling through the thin AlAs layers. From the device development standpoint, it is quite encouraging that this finding runs counter to the usual trend of decreasing  $\kappa$  with decreasing superlattice layer thickness.

## ACKNOWLEDGMENTS

G.C. acknowledges the support of DARPA HERETIC program through JPL and ONR MURI program on thermoelectrics (Grant No. N00014-97-1-0516). Work at NRL was supported by the Office of Naval Research. T.B. acknowledges financial support from the School of Engineering and MANE Department of Rensselaer Polytechnic Institute.

- <sup>1</sup>J. F. Klem, and M. L. Lovejoy, *J. Vac. Sci. Technol. B* **13**, 702 (1995).
- <sup>2</sup>H. K. Choi, C. A. Wang, G. W. Turner, M. J. Manfra, D. L. Spears, G. W. Charache, L. R. Danielson, and D. M. Depoy, *Appl. Phys. Lett.* **71**, 3758 (1997).
- <sup>3</sup>D. Z. Garbuzov, H. Lee, V. Khalfin, R. Martinelli, J. C. Connolly, and G. L. Belenky, *IEEE Photonics Technol. Lett.* **11**, 794 (1999).
- <sup>4</sup>W. W. Bewley *et al.*, *Appl. Phys. Lett.* **76**, 256 (2000).
- <sup>5</sup>R. Werner, T. Bleucl, J. Hofmann, M. Brockhaus, and A. Forchel, *IEEE Photonics Technol. Lett.* **12**, 966 (2000).
- <sup>6</sup>N. Stath, V. Harle, and J. Wagner, *Mater. Sci. Eng., B* **80**, 224 (2001).
- <sup>7</sup>L. Burkle, F. Fuchs, E. Ahlswede, W. Pletschen, and J. Schmitz, *Phys. Rev. B* **64**, 045315 (2001).
- <sup>8</sup>R. Q. Yang, J. L. Bradshaw, J. D. Bruno, J. T. Pham, and D. E. Wortman, *IEEE J. Quantum Electron.* **37**, 282 (2001).
- <sup>9</sup>I. Vurgaftman, J. R. Meyer, and L.-R. Ram-Mohan, *J. Appl. Phys.* **89**, 5815 (2001).
- <sup>10</sup>M. Guden and J. Piprek, *Modell. Simul. Mater. Sci. Eng.* **4**, 349 (1996).
- <sup>11</sup>M. A. Fromowitz, *J. Appl. Phys.* **44**, 1292 (1973).
- <sup>12</sup>B. Abeles, *Phys. Rev.* **131**, 1906 (1963).
- <sup>13</sup>G. Almuneau, E. Hall, T. Mukaiharu, S. Nakagawa, C. Luo, D. R. Clarice, and L. A. Coldren, *IEEE Photonics Technol. Lett.* **12**, 1041 (2000).
- <sup>14</sup>W. Both, A. E. Bochkarev, A. E. Drakin, and B. N. Sverdlov, *Cryst. Res. Technol.* **24**, K161 (1989).
- <sup>15</sup>T. Yao, *Appl. Phys. Lett.* **51**, 1798 (1987).
- <sup>16</sup>G. Chen, C. L. Tien, X. Wu, and J. S. Smith, *J. Heat Transfer* **116**, 325 (1994).
- <sup>17</sup>X. Y. Yu, G. Chen, A. Verma, and J. S. Smith, *Appl. Phys. Lett.* **67**, 3554 (1995); **68**, 1303 (1996).
- <sup>18</sup>W. S. Capinski and H. J. Maris, *Physica B* **219**, 699 (1996).
- <sup>19</sup>T. Borca-Tasciuc, D. Achimov, W. L. Liu, G. Chen, H.-W. Ren, C.-H. Lin, and S. S. Pei, *Microscale Thermophys. Eng.* **5**, 225 (2001).
- <sup>20</sup>S. T. Huxtable, A. Skakouri, C. Labounty, X. Fan, P. Abraham, Y. J. Chiu, J. E. Bowers, and A. Majumdar, *Microscale Thermophys. Eng.* **4**, 197 (2000).
- <sup>21</sup>S. Y. Ren and J. D. Dow, *Phys. Rev. B* **25**, 3750 (1982).
- <sup>22</sup>G. Chen, *J. Heat Transfer* **119**, 220 (1997).
- <sup>23</sup>G. Chen, *Phys. Rev. B* **57**, 14958 (1998).
- <sup>24</sup>S. Tamura, Y. Tanaka, and H. J. Maris, *Phys. Rev. B* **60**, 2627 (1999).

- <sup>25</sup>M. V. Simkin and G. D. Mahan, *Phys. Rev. Lett.* **84**, 927 (2000).
- <sup>26</sup>W. E. Bies, R. J. Radtke, and H. Ehrenreich, *J. Appl. Phys.* **88**, 1498 (2000).
- <sup>27</sup>D. H. Chow, R. H. Miles, T. C. Hasenberg, A. R. Kost, Y.-H. Zhang, H. L. Dunlap, and L. West, *Appl. Phys. Lett.* **67**, 3700 (1995).
- <sup>28</sup>L. J. Olafsen, E. H. Aifer, I. Vurgaftman, W. W. Bewley, C. L. Felix, J. R. Meyer, D. Zhang, C.-H. Lin, and S. S. Pei, *Appl. Phys. Lett.* **72**, 2370 (1998).
- <sup>29</sup>C. Mourad, D. Gianardi, K. J. Malloy, and R. Kaspi, *J. Appl. Phys.* **88**, 5543 (2000).
- <sup>30</sup>C. L. Felix, W. W. Bewley, I. Vurgaftman, L. J. Olafsen, D. W. Stokes, J. R. Meyer, and M. J. Yang, *Appl. Phys. Lett.* **75**, 2876 (1999).
- <sup>31</sup>G. Chen, *J. Heat Transfer* **121**, 945 (1999).
- <sup>32</sup>B. Z. Noshov, W. Barvosa-Carter, M. J. Yang, B. R. Bennett, and L. J. Whitman, *Surf. Sci.* **465**, 361 (2000).
- <sup>33</sup>D. G. Cahill, *Rev. Sci. Instrum.* **61**, 802 (1990).
- <sup>34</sup>T. Borca-Tasciuc, A. R. Kumar, and G. Chen, *Rev. Sci. Instrum.* **72**, 2139 (2001).
- <sup>35</sup>G. Chen, S. Q. Zhou, D. J. Yao, C. J. Kim, X. Y. Zheng, J. L. Liu, and K. L. Wang, *Seventeenth International Conference on Thermoelectrics, Proceedings ICT98* (Cat. No. 98TH8365); 24–28 May, 1998 Piscataway, NJ, p. 202.
- <sup>36</sup>W. Nakwaski, *J. Appl. Phys.* **64**, 159 (1988).
- <sup>37</sup>S. Adachi, *J. Appl. Phys.* **54**, 1844 (1983).
- <sup>38</sup>S. T. Huxtable, *et al.*, *Appl. Phys. Lett.* **80**, 1737 (2002).
- <sup>39</sup>S.-M. Lee and D. G. Cahill, *J. Appl. Phys.* **81**, 2590 (1997).
- <sup>40</sup>G. Chen and T. Zeng, *Microscale Thermophys. Eng.* **5**, 71 (2001).